ChemPubSoc Europe

DOI: 10.1002/cssc.201402721

CHEMSUSCHEM Full Papers

Multielement Crystalline and Pseudocrystalline Oxides as Efficient Catalysts for the Direct Transformation of Glycerol into Acrylic Acid

Alessandro Chieregato,[a, b, d] M. Dolores Soriano,[a] Ester García-González,[c] Giuseppe Puglia,[b] Francesco Basile,[b, d] Patricia Concepción,[a] Claudia Bandinelli,[b] José M. López Nieto,*[a] and Fabrizio Cavani*[b, d]

Glycerol surplus from biodiesel synthesis still represents a major problem in the biofuel production chain. Meanwhile, those in the acrylic acid market are looking for new processes that are able to offer viable alternatives to propylene-based production. Therefore, acrylic acid synthesis from glycerol could be an effective solution to both issues. Among the viable routes, one-pot synthesis theoretically represents the most efficient process, but it is also highly challenging from the catalyst design standpoint. A new class of complex W–Mo–V mixed-oxide catalysts, which are strongly related to the hexagonal tungsten bronze structure, able to directly convert glycerol into acrylic acid with yields of up to 51% are reported.

Introduction

Despite the 2008–2009 global recession, world energy consumption is foreseen to grow with an outstanding 56% increase by 2040, and to satisfy this demand, renewable fuels, together with conventional sources, will play an important role.[1] In this regard, since the early 1990s, biodiesel has been seen by many countries as one of the most favorable choices;[2–4] indeed, in spite of unclear ecological and ethical aspects related to its production,[5] a large amount of money has been invested in the biodiesel sector and current figures are predicted to double by 2020.[6,7] Therefore, hand-in-hand with biodiesel growth, coproduced glycerol represents an abundant bio-based building block for the synthesis of a wide range of chemicals and a crucial economic opportunity to valorize the biofuel production chain. Of the various options for glycerol upgrading, the dehydration process to acrolein is one of the most debated in the literature because this aldehyde is an intermediate molecule for the production of important chemicals such as D,L-methionine and acrylic acid.[6,8–10] In this regard, the one-pot synthesis of acrylic acid from glycerol theoretically allows the production of intermediate acrolein to be avoided; thus restricting toxicity concerns related to this aldehyde and simplifying reactor design and heat exchange. Moreover, it would represent a more sustainable route to (at least partially) substitute the current production of acrylic acid from propylene, the latter obtained from the cracking of naphtha. At the same time, it would also alleviate the influence of increasing propylene price[11] on the final cost of the acid monomer. So far, two different approaches have been taken into consideration for the one-pot synthesis: 1) the utilization of a single multifunctional catalyst with both acid and redox properties,[12–19] or 2) the coupling of two catalysts (dehydrating and oxidizing) as two in-series fixed beds in a single reactor.[20–22] The latter approach is generally accepted to lead to higher yields into acrylic acid, even though serious limitations can derive from being forced to use the same reaction conditions for both catalytic beds. Otherwise, the use of more complicated technologies to overcome this issue (e.g., interstage heat exchange) could severely affect the economic feasibility of the process and its competitiveness to the current propylene-based one. Nevertheless, the multifunctional catalyst approach is very demanding from the catalyst design standpoint, since only fine-tuning of the acid and redox properties of the material allows noteworthy yields of the acid monomer to be obtained. Indeed, few multifunctional materials have so far been demonstrated to be effective catalysts for the direct transformation of glycerol into acrylic acid, that is, $FeVO_4$/Fe_2O_3,[12] Mo–V–O, Mo–V–Te–Nb–O, W–V–(Nb)–O,[13–18] and V-impregnated zeolites.[19] Herein, we report a new class of cata-

[a] A. Chieregato, Dr. M. D. Soriano, Dr. P. Concepción, Prof. Dr. J. M. López Nieto
Instituto de Tecnología Química, UPV-CSIC
Campus de la Universidad Politécnica de Valencia
Avda. Los Naranjos s/n; 46022 Valencia (Spain)
E-mail: jmlopez@itq.upv.es

[b] A. Chieregato, G. Puglia, Dr. F. Basile, C. Bandinelli, Prof. Dr. F. Cavani
Dipartimento di Chimica Industriale
ALMA MATER STUDIORUM Università di Bologna
Viale Risorgimento 4, 40136 Bologna (Italy)
E-mail: fabrizio.cavani@unibo.it

[c] Prof. Dr. E. García-González
Departamento Química Inorgánica, Facultad de Ciencias Químicas
Universidad Complutense, 28040 Madrid (Spain)

[d] A. Chieregato, Dr. F. Basile, Prof. Dr. F. Cavani
Centro Interdipartimentale di Ricerca Industriale "Energia e Ambiente"
ALMA MATER STUDIORUM Università di Bologna
Bologna (Italy)

Supporting Information for this article is available on the WWW under http://dx.doi.org/10.1002/cssc.201402721.

lysts that result in high yields of acrylic acid (up to 51%). The introduction of molybdenum into a tungsten–vanadium mixed oxide creates not only changes in the catalyst structure, but it also leads to a multifunctional material with both Brønsted acid and redox sites, as well as stable oxidizing properties over a wide range of temperatures. The W-Mo-V catalysts presented herein are complex oxides composed of a hexagonal bronze WO_x-type phase and/or a pseudocrystalline phase. We also demonstrate that the combination of the three elements is fundamental for the optimization of glycerol oxidation to give acrylic acid.

Results and Discussion

Physical and chemical properties

To study the influence of tungsten, molybdenum, and vanadium on the catalytic performance and structure of the materials, bicomponent W–Mo and tricomponent W–Mo–V oxide catalysts were synthesized.

Figure 1 shows the XRD patterns of catalysts prepared by heat treatment at 600 °C in nitrogen. For the tricomponent systems with low molybdenum contents (samples WMoV-1 and WMoV-2), XRD maxima can be assigned to a hexagonal tungsten bronze (HTB)-type phase. Interestingly, crystallinity is considerably improved for the sample containing a higher amount of vanadium (WMoV-2); this emphasizes the conclusion formerly drawn by our group that vanadium has a stabilizing effect on the HTB structure.[14] By keeping the W/V ratio constant and increasing the amount of molybdenum (i.e., WMoV-3 and WMoV-4), the XRD patterns are dominated by two diffraction maxima at $2\theta \approx 22$ and 46°, whereas broad diffraction maxima appear at $2\theta \approx 27$, 32, 50, and 55° (Figure 1 c and d). These patterns are similar to those reported for molybdenum- and tungsten-based mixed oxides by Murayama et al.[23] According to these authors, samples with higher molybdenum contents were characterized by two peaks at $2\theta = 22$ and 46° that could be attributed to the (0 0 1) and (0 0 2) planes of a bronze-type frame, which suggested that these materials had a layer-type crystal structure. These diffraction maxima can correspond to the (0 0 1) and (0 0 2) *d* spacing of any structure based on the corner-sharing octahedral ReO_3-like framework with a basic cell parameter of about 3.8 Å. When considering the whole set of diffraction maxima, although ill defined, they are all compatible with the well-known orthorhombic tungsten bronze $Cs_xNb_{2.54}W_{2.46}O_{14}$[24] or the so-called Mo–V–Te–Nb–O M1 phase.[25] Due to the unclear identity of the crystal phases present, the samples were further investigated by electron diffraction and high-resolution electron microscopy. In agreement with XRD data, the tricomponent samples with low Mo content, namely, WMoV-1 and WMoV-2, are composed of crystals of the hexagonal phase, with bigger crystallites in sample WMoV-2 (average size > 100 nm vs. 50–100 nm for WMoV-1). For a high Mo content (i.e., WMoV-3 and WMoV-4), the HTB phase is not stabilized and samples are formed by smaller crystallites (10–50 nm), as shown by the electron-diffraction ring pattern for the WMoV-3 sample (Figure 2 a). The corresponding high-resolution image (Figure 2 b) shows a group of crystals in which lattice fringes are observed at a *d* spacing of about 3.8 Å. The contrast of the image illustrates very well the ill-defined periodicity along the perpendicular direction and disordered packing of structural planes. This poorly resolved structural arrangement is consis-

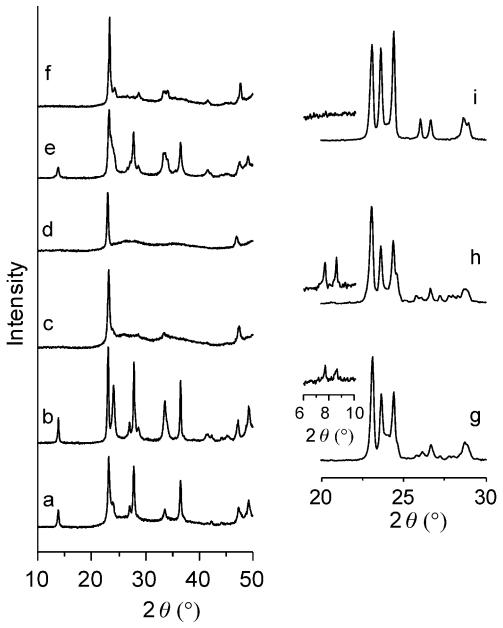

Figure 1. XRD patterns of samples heat treated at 600 °C. Three samples were also heat treated in nitrogen at 800 °C (as indicated in parentheses). a) WMoV-1, b) WMoV-2, c) WMoV-3, d) WMoV-4, e) WMo-1, f) WMo-2; g) WMoV-1[800], h) WMoV-3[800], and i) WMo-2[800].

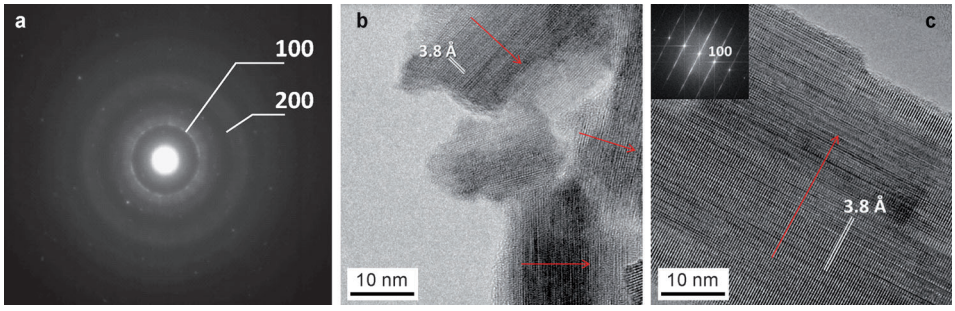

Figure 2. a) Electron-diffraction ring pattern for the WMoV-3 sample. The diagram is formed by diffuse rings and only a sharp ring assigned to the (100) diffraction maximum is observed; (200) can also be distinguished, although with low intensity. b) High-resolution image of crystals of the WMoV-3 sample. Lattice fringes at 3.8 Å can be observed. Red arrows show the disordered stacking of crystal planes. c) High-resolution image of a rod-like crystal of WMo-2. Lattice planes spaced at about 3.8 Å can be observed, as well as disordered contrast along the perpendicular direction. The corresponding Fourier transform has been included as an inset.

tent with the previous interpretation of the corresponding XRD pattern. In the absence of vanadium, the XRD patterns have a strong similarity to those of samples containing vanadium; the tungsten/molybdenum ratio plays a pivotal role in stabilizing the HTB-type phase. Figure 2c shows a rod-like crystal of the WMo-2 sample. Lattice planes equally spaced at about 3.8 Å can be observed along with disordered contrast along the perpendicular direction; moreover, the image contrast is very similar to that in Figure 2b, although the average crystal size is above 100 nm. To facilitate the formation of well-crystallized phases and to help in the elucidation of the nature of these materials, the same catalyst precursors were heat treated in nitrogen at 800 °C (for more details, see the Experimental Section). The XRD patterns of samples heat treated at 800 °C (i.e., WMoV-1[800], WMoV-3[800], and WMo-2[800]) are shown in Figure 1g–i. The three patterns reveal the formation of a monoclinic WO_3-type phase (m-WO_3), in addition to a certain amount of Mo_5O_{14}-type phase in the samples containing vanadium (as shown by peaks at $2\theta \approx 7.7$ and 8.4°). The WMoV-3[800] sample is composed of a m-WO_3-type phase as the major component, which, according to an electron microscopy study (Figure S1a in the Supporting Information), does not contain vanadium; the average atomic composition is $W_{0.7}Mo_{0.3}O_3$. Interestingly, vanadium is segregated into M_5O_{14}-type phase crystals, which constitute the minor component of the sample and their atomic average composition is $(W_{0.64}Mo_{0.3}V_{0.03})_5O_{14}$ (Figure S1b in the Supporting Information).

All of the above results are consistent with the idea that catalysts heat treated at 600 °C are composed of a matrix constructed from corner-sharing MO_6 octahedra and distributed in orderly stacked crystal planes ($d \approx 3.8$ Å). Inside the planes, further structural reconstruction is needed to achieve a particular structural type, as demonstrated by the ill-defined diffraction maxima and disordered contrast of the high-resolution images. Indeed, very specific composition/temperature conditions are required for the formation of the metastable h-WO_x phase.[14,26,27] In this sense, previous structural investigations into the $W_xMo_{1-x}O_3$ system have shown that, in the $0.25 \le x \le 0.70$ composition range, materials adopt the ξ-type phase, which is very similar to that of m-WO_3, although the unit cell is more distorted, with a random distribution of metal atoms in the same space group, $P2_1/n$.[28] The phase appears at room temperature and, for $x < 0.5$, increasing the temperature to between 100 and 420 °C, transforms this phase into γ-WO_3, which is equivalent to pure m-WO_3. Our results show, however, that the monoclinic phase cannot be stabilized below about 800 °C.

FTIR spectra were recorded for W–Mo and W–Mo–V catalysts (Figure 3). Both vanadium-free and vanadium-containing

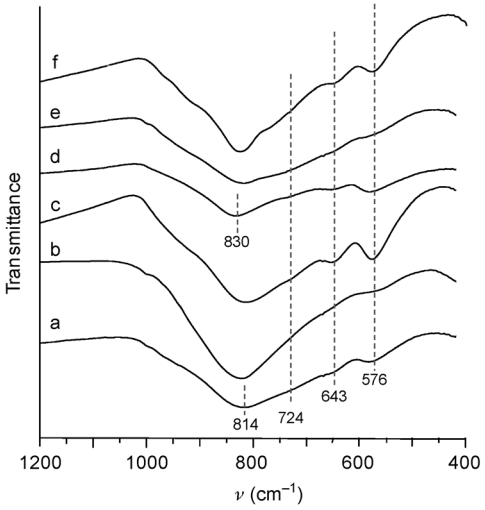

Figure 3. FTIR spectra of samples heat treated at 600 °C: a) WMoV-1, b) WMoV-2, c) WMoV-3, d) WMoV-4, e) WMo-1, and f) WMo-2.

samples are similar. A broad band centered between $\tilde{\nu} = 814$ and 830 cm^{-1} can be assigned to W–O–W(Mo) stretching, whereas the band at $\tilde{\nu} = 724$ cm^{-1} should be related to W–O–V; bands at $\tilde{\nu} = 643$ and 576 cm^{-1} may be associated with W–O–W and W–O–V rocking vibrations and Mo–O–X (X = W or V).[29,30] Therefore, a strong similarity between the spectra is consistent with the above structural description in which all catalysts have a more or less regular distribution of corner-sharing octahedra in the HTB or pseudocrystalline structure from the M–O–M vibrations observed.

The specific surface areas of the catalysts are shown in Table 1; the higher vanadium contents in samples with the HTB-type structure (WMoV-1 and WMoV-2) result in lower BET surface areas, as a consequence of higher crystallinity and larger average crystal size; this is in agreement with our previous results on WV catalysts.[14] For samples containing the pseudocrystalline phase (WMoV-1 vs. WMoV-3, or WMoV-2 vs. WMoV-4), the higher molybdenum content allows a significant increase in the specific surface area to be obtained; the effect is more relevant when vanadium content is higher.

Table 1. Main physicochemical features of W–Mo and W–Mo–V oxides.

Sample	W/Mo/V[a]		S_{BET}	NH_3-TPD[b]		B/L[c]
	gel	catalyst[d]	[$m^2 g^{-1}$]	[$\mu mol_{NH_3} g^{-1}$]	[$\mu mol_{NH_3} m^{-2}$]	
WMo-1	1:0.2	1:0.19:0	26	150.9	5.8	13
WMo-2	1:0.6	1:0.52:0	13	47.9	3.7	18
WMoV-1	1:0.3:0.1	1:0.22:0.06	30	91.1	3.0	22
WMoV-2	1:0.2:0.2	1:0.28:0.17	12	34.8	2.9	28
WMoV-3	1:0.5:0.1	1:0.45:0.04	38	129.0	3.4	18
WMoV-4	1:0.5:0.2	1:0.86:0.14	22	114.3	5.2	20
WV[e]	1:0:0.23	1:0:0.21	21	76	3.7	n.d.[f]

[a] Atomic ratios; W is equal to unity. [b] NH_3-TPD = temperature-programmed desorption of ammonia. [c] Ratio between the mass-normalized areas of ammonia peaks relative to its adsorption (at 25 °C) on Brønsted (B) or Lewis (L) acid sites. [d] Experimental data obtain by SEM/energy-dispersive X-ray spectroscopy (EDS) analysis. [e] Sample reported as WV-3 in Ref. [9]. [f] n.d. = not determined.

A similar comparison can be performed when characterizing the acid sites (see Table 1). The addition of molybdenum leads to a remarkable decrease in the overall acidity (see WMo-1 and WMo-2), both on mass and surface area bases; however, Brønsted acidity increases. A similar trend is displayed for HTB-like samples (WMo-1, WMoV-1, and WVMo-2): the introduction of vanadium decreases the total acidity (more pronounced on a mass basis), but it increases the ratio of Brønsted/Lewis acid sites.

Moreover, the augmented molybdenum content in the pseudocrystalline structures (WMo-2, WMoV-3, and WMoV-4) brings about an increase in total acidity, but it suppresses the presence of Brønsted-type acid sites. This evidence shows that the introduction of redox elements (i.e., vanadium and molybdenum) into the WO_3 framework also plays a role in the nature of acid sites. Overall, it is important to note that all of the mixed oxides studied have a predominantly Brønsted acid character; therefore, emphasizing the role played by these acid sites in the glycerol dehydration step.[31,32]

Glycerol oxydehydration

The catalytic behavior of every sample was studied in the temperature range 270–410 °C and at different residence times. For all of the catalysts and reaction conditions explored, complete conversion of glycerol was always obtained, as also reported for W–V–Nb–O catalysts.[15,17] Even at a very low contact time, polyol conversion did not decrease due to the formation of oligomers and ketals (generally grouped together as "heavy compounds"). From the product trends reported herein (see below), it is evident that the same phenomenon is also present for all of the catalysts studied. Moreover, as far as the nature of these compounds is concerned, a detailed characterization has already been reported.[17] However, it is worth mentioning that the same kinds of compounds were also detected among the reaction products of the catalysts studied herein at low contact times and/or low reaction temperatures.

Catalytic trends at a constant molar ratio of feed

Table 2 provides a summary of some of the catalytic results obtained in the oxydehydration of glycerol performed on bicomponent W–Mo and tricomponent W–Mo–V catalysts. Moreover, Table S1 in the Supporting Information lists representative reactivity results for each catalyst. Generally speaking, both bicomponent catalysts showed complete glycerol conversion and remarkable acrolein yield; however, only low yields in partial oxidation products (mainly acrylic and acetic acid) were obtained, along with high yields in both heavy compounds and CO_x. At a contact time of 0.4 s at 330 °C, WMo-2 (which showed a better catalytic performance than that of WMo-1) allowed an acrylic acid selectivity of 12% to be obtained, along with 28% acrolein (Figure 4). The highest heavy compounds selectivity (35%) was reached at 270 °C; thus decreasing in favor of carbon oxides at higher temperatures. The relevant formation of heavy compounds, particularly for WMo-1, can be attributed to the low ratio of Brønsted/Lewis acid sites; indeed, poor Brønsted acid properties are known to bring about partial glycerol dehydration into 1-hydroxyacetone and allylic alcohol, finally favoring successive ketalization.[15] Moreover, acrolein can also generate heavy compounds by both self-oligomerization and ketalization thorough condensation with glycerol; the latter reactions are catalyzed by the same acid sites as those needed for the first step of glycerol dehydration.[17] Therefore, since molybdenum alone is clearly inefficient in the fast oxidation of acrolein (as underlined by the high ratio between acrolein and acrylic acid, even for high molybdenum loadings in the catalyst; see WMo-2), parallel reactions taking place from the abovementioned molecules, and leading to heavy compounds, are favored.

A remarkable improvement in the oxidation of acrolein to acrylic acid is observed for the tricomponent samples W–Mo–V–O, providing the well-known redox features of vanadium in oxidation catalysis. The introduction of vanadium in the oxide structure, even at low concentration, for example, WMoV-1, led to a remarkable difference in the catalytic performance. Indeed, at low temperature, the acrylic acid selectivity increased almost three times (from 7 to 18%) and its maximum shifted from 330 to 270 °C; this indicates the superior redox properties of vanadium to those of molybdenum; on the other hand, upon increasing the temperature, total combustion was favored. Catalyst WMoV-3 is the material that gave the highest acrylic acid selectivity (31%) at the lowest temperature. The heavy compounds selectivity was between 7 and 12% and the CO_x selectivity varied from 40 to 50%. At temperatures higher than 330 °C, the acrylic acid selectivity decreased, partially in favor of carbon oxides, but, to some extent, also in favor of acrolein and heavy compounds; this suggests that, at higher temperature, oxygen introduced in the feed is not enough to

Table 2. Structure–reactivity correlations for the productivity (P) for acrylic acid (AA) and acrolein (A).[a]

Sample	Structure[b]	Maximum AA selectivity ($T \leq 330$ °C)[c]		P [$g_{product}\,h^{-1}\,g_{CT}^{-1}$][d]		P [$g_{product}\,h^{-1}\,m_{CT}^{-2}$) × 10^2][e]	
		$\tau = 0.15$ s	$\tau = 0.4$ s	AA	A	AA	A
WMo-1	HTB	n.d.	5 (330)	0.008	0.021	0.032	0.080
WMo-2	Ps-C	5 (330)	12 (330)	0.040	0.11	0.31	0.86
WMoV-1	HTB	14 (310)	16 (290)	0.055	0.048	0.18	0.16
WMoV-2	HTB	14 (330)	21 (330)	0.059	0.070	0.49	0.58
WMoV-3	Ps-C	17 (290)	31 (290)	0.12	0.023	0.31	0.060
WMoV-4	Ps-C	28 (330)	20 (330)	0.066	0.053	0.30	0.24

[a] All of the values reported were obtained with a feed molar ratio for oxygen/glycerol/water/nitrogen of 4:2:40:54. Glycerol conversion was always complete. [b] Overall crystalline structure of the sample. Ps-C: pseudocrystalline. [c] Maximum acrylic acid selectivity obtained at a temperature lower than 330 °C at contact times of 0.15 and 0.4 s. The temperature at which the maximum yield was observed is reported in parentheses. [d] Productivity calculated as $g_{AA}\,h^{-1}\,g_{CT}^{-1}$ or $g_A\,h^{-1}\,g_{CT}^{-1}$ (i.e., h^{-1}). Reaction conditions: feed 290 °C, contact time 0.4 s. [e] Productivity calculated as $g_{AA}\,h^{-1}\,m_{CT}^{-2}$ or $g_A\,h^{-1}\,m_{CT}^{-2}$. For graphical reasons, these values are multiplied by 10^2. Reaction conditions: 290 °C, contact time 0.4 s.

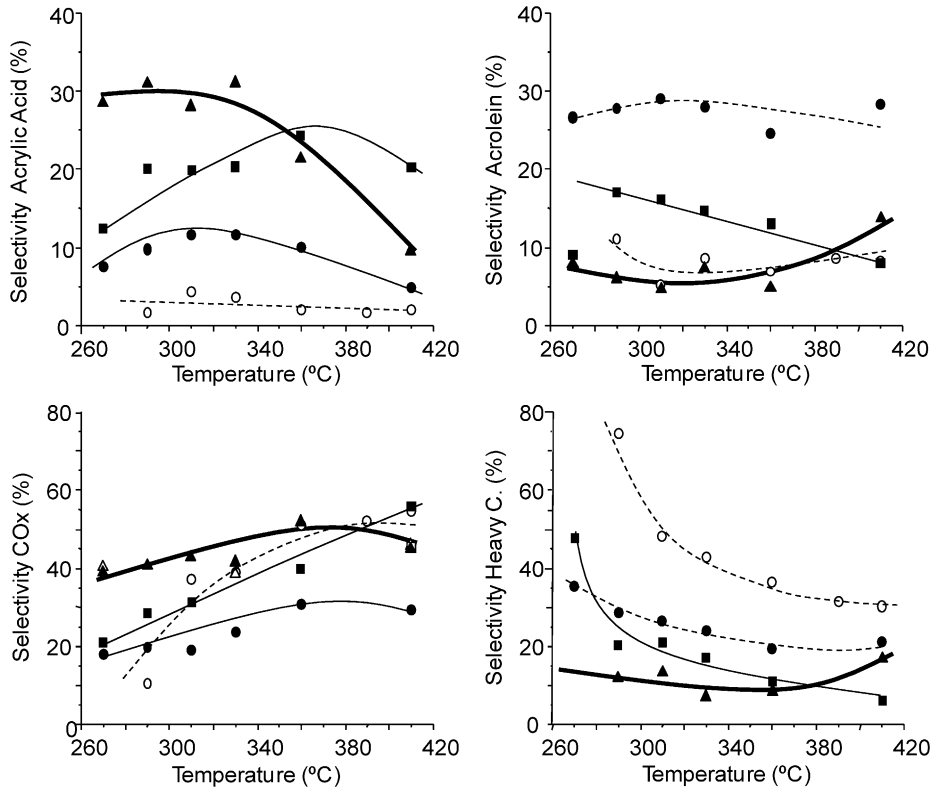

Figure 4. Variation of selectivity to the main reaction products as a function of reaction temperature obtained for glycerol transformation on different catalysts: WMo-1 (○), WMo-2 (●), WMoV-3 (▲), and WMoV-4 (■). In all cases, a glycerol conversion of 100% was achieved.

oxidize acrolein. All in all, a remarkable note for the catalytic performance of WMoV-3 is that the acrylic acid selectivity is almost identical across a wide range of temperatures (from 270 to 330 °C). By comparing this catalyst with those reported in the literature for the same reaction (see above), it is evident that this behavior represents an important step forward for the design of catalysts that are more suitable for industrial scaleup. Indeed, in oxidation catalysis, the precise control of temperature along the entire fixed-bed reactor length represents a very challenging task at the industrial scale.

Thus, the combination of molybdenum and vanadium leads to better control of the oxidative properties of the catalysts to smooth the oxidizing strength of vanadium. In regard to acrylic acid selectivity as a function of temperature, a similar trend to that observed for WMoV-3 was recorded for WMoV-4, but at a lower contact time (0.15 s; Figure S2B in the Supporting Information). Indeed, from 270 to 410 °C, the acrylic acid yield varied by only a few percent from 22 to 28%. Moreover, at low temperature, the carbon oxide yields were much lower, even if there was no gain in acrylic acid yield, since the difference is essentially accounted for in the formation of more heavy compounds. However, when comparing WMoV-3 and WMoV-4 tested at a contact time of 0.15 s (Figure S2 in the Supporting Information), the latter leads to higher yields of acrylic acid and lower yields of CO_x. Finally, when comparing WMoV-3 and WMoV-4 tested at a contact time of 0.4 s (Figure 4), higher acrylic acid yields were obtained for the former as lower yields of acrolein and much lower yields of heavy compounds, corresponding to higher CO_x yields. In conclusion, higher loadings of vanadium improve the oxidation process, but lead to total oxidation products at higher temperatures and residence times; on the other hand, high amounts of molybdenum suppress both selective glycerol dehydration and acrolein oxidation to favor parallel reactions that lead to heavy compounds.

Productivity

Because of the wide range of physicochemical properties of the complex oxide catalysts reported herein, we calculated the productivity for acrylic acid and acrolein (Table 2). Productivity can reveal differences with regard to the active phases; therefore, making it possible to relate the catalytic performance and nature of the catalyst. By comparing samples WMoV-1 and WMoV-2, both with the HTB structure, it is possible to determine the role of vanadium in the catalysts; indeed, on a similar basis to that of molybdenum, the sample richer in vanadium (WMoV-2) improves the productivity not only for the partial oxidation product, but also for acrolein. This evidence indicates once again the role of vanadium in acrolein oxidation, and it also reflects that a fast oxidation step is mandatory to limit the parallel reaction that leads to heavy compounds. Molybdenum is also crucial in the oxidation process; indeed, moving from WMoV-1 to WMoV-3 (with a similar amount of vanadium, but higher content of molybdenum), acrylic acid productivity is greatly improved. Moreover, the higher amount of molybdenum (WMoV-4 vs. WMoV-2) leads to a variation in the distribution of the elements and in the nature of the acid sites (from Brønsted to Lewis), which suppress the overall oxydehydration process, as highlighted by the abrupt overall productivity drop (for acrylic acid + acrolein) per square meter of catalyst. On the other hand, acrylic acid productivity on a molar basis increases from 0.059 to 0.066 h^{-1} due to the increased surface area (from 12 to 22 $m^2 g^{-1}$).

The role of the crystal structure can also be outlined from productivity trends calculated on the basis of mass and surface area. For the tri-component catalysts, the AA productivity trend has its maximum located in different positions if calculated either based on mass or surface area, that is, WMoV-3 and WMoV-2, respectively. This means that the best catalyst, in terms of productivity per specific surface area, is WMoV-2; however, because of its low area, productivity remains scarce

on the basis of mass. Therefore, the pseudocrystalline structure for low vanadium and high molybdenum contents plays an important role in the productivity of the catalysts per gram of catalyst. On the other hand, the relative distribution of the elements appears to have a major impact on the catalytic performance: productivity depends on the oxide composition, whether it is in the HTB or pseudocrystalline phase.

For bicomponent (W–Mo) catalysts, acrylic acid productivity is relatively high due to the low surface area; however, it is low per gram of catalyst. Moreover, the high overall acrolein productivity underlines the insufficient redox properties of vanadium-free catalysts (acrolein remains mainly unconverted). Finally, to gain a wider picture of the role of tungsten, it is of interest to compare our results with those recently published by Shen et al.,[18] who used Mo/V oxides (without tungsten), prepared by slurry synthesis (i.e., $Mo_6V_9O_{40}$ and MoO_3 phases) with relatively low surface areas (10–12 $m^2 g^{-1}$). When glycerol was made to react on these oxides, low carbon balances were obtained due to the poor acid properties of the catalysts (both as total acidity and likely as the ratio of Brønsted/Lewis acid sites), as well as a wide range of C_3 and C_2 products.

Therefore, the abovementioned results for the W–Mo and W–Mo–V catalysts highlight that 1) a high number of Brønsted acid sites are needed to perform the glycerol dehydration step selectively in give acrolein, which emphasizes the fundamental role of tungsten; 2) the specific productivity of the catalysts is governed by the abundance of the elements in the oxide frame, whether it is composed of the HTB or pseudocrystalline structure; and 3) the pseudocrystalline structure only has a role in determining the catalyst productivity due to its influence on the surface area.

Influence of the feed composition and time on stream

The catalytic performance of WMoV-3 was studied as a function of inlet feed composition because it gives the highest acrylic acid yield and productivity at the lowest temperature and it is stable over a wide range of temperatures. Indeed, we recently reported that a high oxygen partial pressure enhanced the reoxidation process of the catalyst and boosted the selectivity of the partial oxidation product (acrylic acid).[17] Moreover, to prove the beneficial effect of molybdenum on the oxidation step, we also analyzed the catalytic behavior of the WV oxide catalyst under the same reaction conditions (see Table 1) that showed the best catalytic performance under a molar ratio of oxygen/glycerol feed of 4:2.[14] These catalytic tests were carried out at a contact time close to 0.4 s and 290 °C for the best balance between the partial oxidation of acrolein into acrylic acid and its total combustion into carbon oxides for a maximum yield of acrylic acid (Figure S3 in the Supporting Information and Refs. [9,10]). In the catalytic tests presented in Figure 5a and b, glycerol and water molar ratio in feed were kept constant, 6 and 40%, respectively. Meanwhile, the oxygen and inert gas partial pressures were changed to vary the oxygen molar ratio and keep the overall contact time constant. Generally speaking, excluding the oxygen/glycerol molar ratio of 6:6, it is evident that WMoV-3 (Figure 5a) is much more efficient in the partial oxidation of acrolein into acrylic acid than WV (Figure 5b). Indeed, acrylic acid increases at a much higher pace; moreover, the acrylic acid/acrolein ratio is substantially higher.

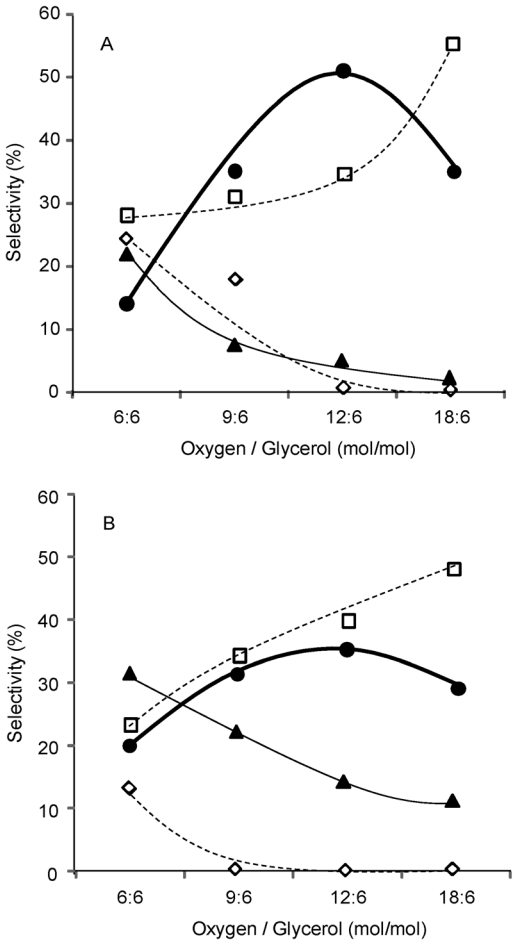

Figure 5. Main reaction products for glycerol oxydehydration on WMoV-3 (A) and WV (B), as a function of the molar ratio of the oxygen feed. Glycerol and water molar ratio constants of 6 and 40%, respectively. Contact time 0.4 s. Glycerol conversion was always complete for both catalysts. Selectivity to acrylic acid (●), acrolein (▲), heavy compounds (◇), and CO_x (□). Minor products detected were acetic acid and acetaldehyde as well as traces of unknown compounds.

At an oxygen/glycerol molar ratio of 12:6, WV reached only an acrylic acid selectivity of 35%, whereas WMoV-3 reached 51%. Notably, the acrylic acid yield for the tricomponent catalyst is one of the highest values reported so far in the literature for the one-pot synthesis of acrylic acid from glycerol by using a single multifunctional catalyst. Interestingly, the poorest catalytic performance of WMoV-3 compared with WV was obtained at an oxygen/glycerol molar ratio of 6:6; indeed, it is evident from the higher formation of heavy compounds and lower acrylic acid selectivity. This phenomenon can be ascribed to the higher acidity of the molybdenum-containing catalyst (76 vs. 129 $\mu mol_{NH_3} g_{cat.}^{-1}$); the properties of the latter have a greater influence on the formation of heavy compounds when the oxidation step is slower. Indeed, it can be inferred that if the oxidation step is slow, higher acidity impedes the fast desorption of intermediate acrolein; therefore, favoring the parallel

reaction that leads to heavy compounds. Overall, it is worth mentioning that oxygen conversion for both catalysts constantly decreases as a function of oxygen concentration (Table S3 in the Supporting Information). However, in the case of WMoV-3, oxygen conversion is always higher, which suggests that the presence of molybdenum eases the oxidation process, making it possible to reach higher acrylic acid yields.

Very similar catalytic behavior was also observed for both catalysts when the oxygen/glycerol molar ratio was set to two (Figure S4 A and B in the Supporting Information). The yield of heavy compounds decreased, mainly in favor of acrylic acid rather than CO_x. Therefore, high partial pressures of oxygen play a fundamental role in accelerating the catalyst re-oxidation process. When acrolein was made react on WMoV-3 under the same reaction conditions (Figure 6), different behavior was observed because increasing the partial pressure of both oxygen and glycerol, but keeping their ratio constant, decreased the acrylic acid selectivity in favor of carbon oxides. Finally, upon getting closer to the flammability point (ratio 6:18), the total oxidation of acrolein to CO_x is increased. In summary, by comparing these trends with those obtained for glycerol and the different CO_x yields from the two experiments, it can be inferred that glycerol strongly interacts with the catalyst and leading to saturation of the surface. As a consequence of these results, we can determine that 1) the availability of the redox sites is limited, which implies the need for a high partial pressure of O_2 to guarantee a sufficient concentration of oxidizing sites, and 2) the glycerol residence time on the catalyst surface is augmented, leading to its direct oxidation (Scheme 1).

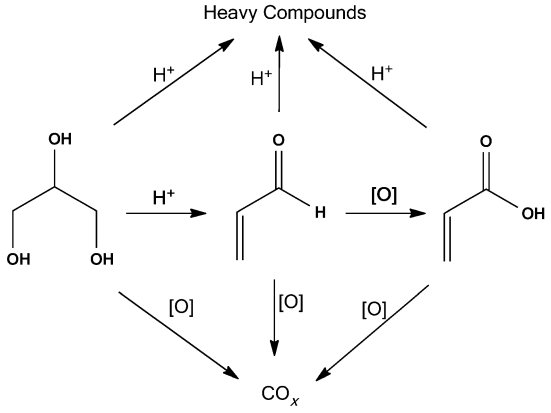

Scheme 1. Main reaction scheme for glycerol oxydehydration. The acid sites (H^+) and redox sites ([O]) catalyze both the formation of acrylic acid and parallel reactions that lead to byproducts.

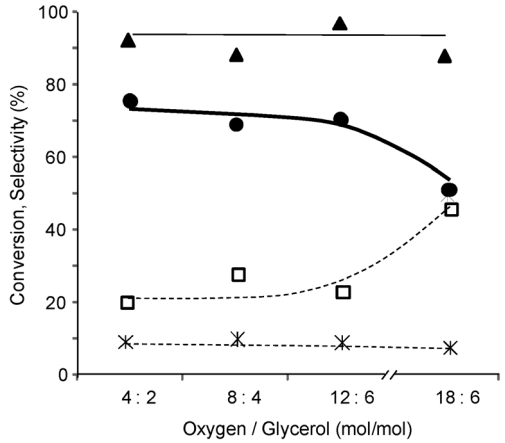

Figure 6. Main reaction products for acrolein oxidation on WMoV-3 as a function of the molar ratio of the oxygen/acrolein feed. The water molar ratio was constant at 40%. Acrolein conversion (▲); selectivity to acrylic acid (●), CO_x (□), and others (*; mainly acetic acid and acetaldehyde).

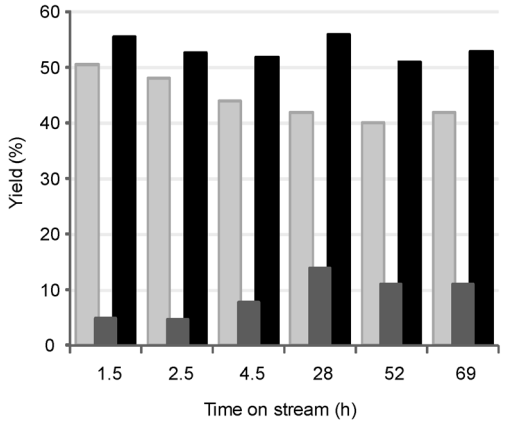

Figure 7. ToS tests for glycerol oxydehydration on WMoV-3. The molar ratio of the glycerol/O_2/H_2O/N_2 feed was 6:12:40:42. The glycerol conversion was always complete. Yields are given for acrylic acid (■), acrolein (■), and the sum of acrylic acid and acrolein (■).

Finally, the catalytic behavior of WMoV-3 was studied as a function of the time on stream (ToS; Figure 7) by using the same reaction conditions as those for which the maximum acrylic acid yield was obtained. After 70 h ToS, the glycerol conversion was always complete and the sum of acrolein and acrylic acid was constant with an average value of around 53% and an initial acrylic acid yield of 51%. On the other hand, after 90 min ToS (i.e., the time normally used to study the behavior of the catalysts; see the Experimental Section), the acrylic acid yield slowly started to decrease in favor of the aldehyde. Overall, after about 28 h ToS, both product yields reached stable average values of 42 (acrylic acid) and 12% (acrolein), which were stable for at least the next 40 h. By comparing the XRD spectra of fresh and spent samples after 69 h ToS (Figure S5 in the Supporting Information), it is possible to see that a new diffraction peak appears at $2\theta \approx 26^\circ$; this is most likely to be related to partial decomposition of the pseudocrystalline structure into m-WO_3. Moreover, by comparing the Raman spectra of fresh and spent catalysts (Figure S6 in the Supporting Information), the presence of carbonaceous deposits on the surface is revealed. Both phenomena could thus be attributed to the changes in product distribution during the ToS tests. To assess the relative importance of the two phenomena, an attempt at regeneration was carried out by feeding a mixture of oxygen and nitrogen (molar ratio 5:95) at

350 °C for 2 h with a contact time 0.4 s. As demonstrated by recording the Raman spectra of the regenerated catalyst (Figure S6 in the Supporting Information), the carbon deposits were effectively removed by the oxidation treatment; on the other hand, once the regenerated catalyst was used to continue the ToS test, the improvement in acrylic acid selectivity was minimal (increase of 2–3%). Hence, the change in the crystalline phase is clearly the key-factor that governs catalyst deactivation. By comparing the variation observed for the crystal structure of the W–Mo–V catalyst to that of W–V–Nb oxide previously studied,[12] the stabilizing role played by niobium is evident; indeed, after an analogous ToS test, the structure of the niobium-containing catalyst was preserved. This evidence suggests that niobium might play a similar role in both pseudocrystalline and HTB structures, as reported for the M1 phase in Mo–V–Nb–Te catalysts.[20]

Conclusions

Glycerol oxydehydration on a single catalyst is a challenging process from the standpoint of catalyst design. In this study, a new class of complex W–Mo–V oxides, strongly related to HTBs, were investigated. The physicochemical properties and catalytic performance made the main role of each element in the oxide framework clear: tungsten dehydrated glycerol to form acrolein, vanadium oxidized acrolein to form acrylic acid, and molybdenum moderated the strong oxidizing properties of vanadium. The atomic ratio of the elements was pivotal for tuning the redox and acid properties, but it also played a role both in the size of the crystals and in their long-range distribution, and finally influenced the productivity of the catalysts. High oxygen feed molar ratios helped the catalyst in the re-oxidation step and allowed an acrylic acid yield as high as 51% to be obtained on the WMoV-3 catalyst, whereas the molybdenum-free sample (i.e., WV) did not exceed 35% yield of the acid monomer. Acrolein oxidation tests provided evidence that direct oxidation of glycerol and acrolein also took place. ToS tests (ca. 70 h) on WMoV-3 revealed a stable overall yield for acrolein and acrylic acid. Under the reaction conditions studied, the evolution of the crystal phase led to a slight inversion in the yields of the two consecutive products along the first 5 h ToS. However, stable catalytic behavior was observed for more than 40 h ToS.

Experimental Section

Synthesis

The W–V–Mo catalysts were prepared hydrothermally from gels obtained from aqueous solutions of the corresponding salts: ammonium metatungstate hydrate ($\geq$85 wt% WO_3, Sigma–Aldrich), vanadium(IV) oxide sulfate hydrate ($\geq$99.99%, Sigma–Aldrich), and ammonium heptamolybdate tetrahydrate (guaranteed reagent (GR) for analysis, Merck). The hydrothermal synthesis was carried out at 175 °C for 48 h; then the solid was washed and dried at 100 °C overnight. We refer to the dried solid as the catalyst precursor. Lastly, the catalyst precursor was heat treated in N_2 at 600 °C for 2 h. For selected analyses, the catalyst precursor was heat treated in N_2 at 800 °C for 2 h. In this case, the unconventional heat treatment is specifically reported.

Characterization

Surface areas were obtained from N_2 adsorption isotherms by using the BET method; a Micromeritics ASAP 2000 instrument was used. Samples were degassed in situ under vacuum at 250 °C.
Powder XRD patterns were collected by using a PANalytical X'Pert PRO diffractometer with $Cu_{K\alpha}$ radiation and an X'Celerator detector in Bragg–Brentano geometry.
Quantitative EDS analysis was performed by using an Oxford LINK ISIS system attached to a JEOL 6300 electron microscope with the SEMQUANT program, which introduced the ZAF correction. The counting time was 100 s for major and minor elements.
IR spectra were recorded at room temperature in the $\tilde{\nu}$ = 300–4000 cm^{-1} region with a Nicolet 205xB spectrophotometer equipped with a data station at a spectral resolution of 1 cm^{-1} and accumulations of 128 scans. Raman spectra were obtained with an inVia Renishaw spectrometer, equipped with an Olympus microscope. The exciting wavelength was 514 nm from a Renishaw HPNIR laser with a power of approximately 15 mW on the sample.
The NH_3-TPD experiments were carried out on a TPD/2900 apparatus from Micromeritics. A 0.30 g sample was pretreated in a stream of He at 450 °C for 1 h. Ammonia was chemisorbed by pulses at 100 °C until equilibrium was reached. Then, the sample was fluxed with a He stream for 15 min, prior to increasing the temperature to 500 °C in a 100 mL min^{-1} stream of He at a heating rate of 10 °C min^{-1}. The NH_3 desorption was monitored with a thermal conductivity detector (TCD) and a mass spectrometer by following the characteristic mass of ammonia at 15 a.m.u.
Samples for TEM were ultrasonically dispersed in *n*-butanol and transferred to carbon-coated copper grids. Selected-area electron diffraction and high-resolution TEM were carried out on a JEOL JEM3000F electron microscope (point resolution of 0.17 nm). Crystal by crystal EDS microanalysis was performed by using the same microscope equipped with an X-ray microanalysis ISIS 300 (Oxford Instruments) system with a detector model LINK "Pentafet" (resolution 135 eV).

Reactivity experiments

Reactivity experiments for glycerol and acrolein transformations were carried out by using a continuous-flow reactor made of glass, operating at atmospheric pressure. For each condition, all reaction parameters are listed in each figure. A catalyst amount ranging from 0.10 to 0.30 g was loaded in powder form. Residence time (calculated as the ratio between catalyst volume (mL) and total gas flow (mL s^{-1}); the latter was measured at room temperature) was varied. Inlet feed molar ratios between reactants were also changed according to the desired compositions. Unless specified otherwise, the catalytic results were obtained after 90 min of reaction time.
For both glycerol oxydehydration and acrolein oxidation, the effluent stream was bubbled through two in-series abatement devices, which were filled with water (but in some cases anhydrous acetone was used for the identification of compounds that were less soluble in water) and held at a temperature of 0–2 °C; a third refrigerated condenser was left without any solvent. After this abatement, the gaseous stream, still containing oxygen and carbon oxides, was fed into an automatic sampling system for gas chromatography (GC-TCD) analysis. The aqueous solution containing unconverted glycerol and reaction products was analyzed by GC with a Hew-

lett–Packard 5890 instrument equipped with a flame ionization detector (FID). A semicapillary wide-bore OV 351 (polyethyleneglycol treated with terephthalic acid) column was used for the separation of condensed compounds.[12] Two wide-bore columns were used for the separation of noncondensable products: a 5 Å molecular sieves for oxygen and CO, and a Silica Plot for CO_2 (oven temperature 80 °C). Compounds were identified by means of both GC–MS and the injection of pure reference standards for the comparison of retention times in the GC column. A few unknown compounds were eluted in the GC column; we attributed the same response factor to these compounds as the corresponding known compound with the closest retention time. Cyclic ethers were also sometimes produced; however, because it was not possible to perfectly resolve each peak corresponding to cyclic ethers with the chromatographic setup used, both the cyclic ethers and heaviest compounds not eluted from the GC column (left as residues on both the catalyst surface and reactor walls) were quantified as the remainder of the total carbon balance and labeled as heavy compounds.

Acknowledgements

The authors from the Instituto Tecnologia Quimica would like to thank the Spanish Government (Project CTQ2012-37925-C03-1 and program Severo Ochoa SEV-2012-0267) for financial support. CIRI Energia e Ambiente ALMA MATER STUDIORUM, Università di Bologna, is acknowledged for the grant to A.C. E.G.G. acknowledges financial support from the Spanish Government through the project MAT2010-19837-C06-05.

Keywords: biofuels · heterogeneous catalysts · molybdenum · tungsten · vanadium

[1] U.S. Energy Information Administration, *International Energy Outlook* **2013**.
[2] C. A. G. Quispe, C. J. R. Coronado, J. A. Carvalho, Jr., *Renewable Sustainable Energy Rev.* **2013**, *27*, 475 – 493.
[3] E. Gusciute, G. Devlin, F. Murphy, K. McDonnell, *WIREs Energy Environ.* **2014**, *3*, 310 – 322.
[4] S. Kumar, P. Shrestha, P. A. Salam, *Renewable Sustainable Energy Rev.* **2013**, *26*, 822 – 836.
[5] J. P. W. Scharlemann, W. F. Laurance, *Science* **2008**, *319*, 43 – 44.
[6] B. Katryniok, S. Paul, F. Dumeignil, *ACS Catal.* **2013**, *3*, 1819 – 1834.
[7] A. Lind, E. Rosenberga, P. Seljom, K. Espegren, A. Fidje, K. Lindberg, *Energy Policy* **2013**, *60*, 364 – 377.
[8] B. Katryniok, S. Paul, V. Belliere-Baca, P. Reye, F. Dumeignil, *Green Chem.* **2010**, *12*, 2079 – 2098.
[9] B. Katryniok, S. Paul, M. Capron, F. Dumeignil, *ChemSusChem* **2009**, *2*, 719 – 730.
[10] L. Liu, X. Philip Ye, J. J. Bozell, *ChemSusChem* **2012**, *5*, 1162 – 1180.
[11] F. Cavani, N. Ballarini, A. Cericola, *Catal. Today* **2007**, *127*, 113 – 131.
[12] F. Wang, J. Xu, J.-L. Dubois, W. Ueda, *ChemSusChem* **2010**, *3*, 1383 – 1389.
[13] J. Deleplanque, J.-L. Dubois, J.-F. Devaux, W. Ueda, *Catal. Today* **2010**, *157*, 351 – 358.
[14] M. D. Soriano, P. Concepción, J. M. López Nieto, F. Cavani, S. Guidetti, C. Trevisanut, *Green Chem.* **2011**, *13*, 2954 – 2962.
[15] A. Chieregato, F. Basile, P. Concepción, S. Guidetti, G. Liosi, M. D. Soriano, C. Trevisanut, F. Cavani, J. M. López Nieto, *Catal. Today* **2012**, *197*, 58 – 65.
[16] K. Omata, K. Matsumoto, T. Murayama, W. Ueda, *Chem. Lett.* **2014**, *43*, 435 – 437.
[17] A. Chieregato, M. D. Soriano, F. Basile, G. Liosi, S. Zamora, P. Concepción, F. Cavani, J. M. López Nieto, *Appl. Catal. B* **2014**, *150 – 151*, 37 – 46.
[18] L. Shen, H. Yin, A. Wang, X. Lu, C. Zhang, *Chem. Eng. J.* **2014**, *244*, 168 – 177.
[19] C. F. M. Pestana, A. C. O. Guerra, B. F. Glaucio, C. C. Turci, C. J. A. Mota, *J. Braz. Chem. Soc.* **2013**, *24*, 100 – 105.
[20] A. Witsuthammakul, T. Sooknoi, *Appl. Catal. A* **2012**, *413*, 109 – 116.
[21] M. Massa, A. Andersson, E. Finocchio, G. Busca, F. Lenrick, L. R. Wallenberg, *J. Catal.* **2013**, *297*, 93 – 109.
[22] R. Liu, T. Wang, D. Cai, Y. Jin, *Ind. Eng. Chem. Res.* **2014**, *53*, 8667 – 8674.
[23] T. Murayama, N. Kuramata, S. Takatama, K. Nakatani, S. Izumi, X. Yi, W. Ueda, *Catal. Today* **2012**, *185*, 224 – 229.
[24] T. E. Weirich, J. Portillo, G. Coxd, H. Hibste, S. Nicolopoulos, *Ultramicroscopy* **2006**, *106*, 164 – 175.
[25] J. M. López Nieto, P. Botella, M. I. Vázquez, A. Dejoz, *Chem. Commun.* **2002**, 1906 – 1907.
[26] M. Figlarz, *Prog. Solid State Chem.* **1989**, *19*, 1 – 46.
[27] P. Labbe, *Key Eng. Mater.* **1992**, *68*, 293 – 340.
[28] E. Salje, R. Gehlig, K. Viswanathan, *J. Solid State Chem.* **1978**, *25*, 239 – 250.
[29] P. Botella, J. M. López Nieto, B. Solsona, *Catal. Lett.* **2002**, *78*, 383 – 387.
[30] F. Cariati, J. C. J. Bart, A. Sgamelloti, *Inorg. Chim. Acta* **1981**, *48*, 97 – 103.
[31] R. Liu, T. Wang, C. Liu, Y. Jin, *Chin. J. Catal.* **2013**, *34*, 2174 – 2182.
[32] M. Massa, A. Andersson, E. Finocchio, G. Busca, *J. Catal.* **2013**, *307*, 170 – 184.

Received: July 22, 2014
Revised: August 28, 2014
Published online on December 8, 2014